PHYSICAL REVIEW B **79**, 100407(R) (2009)

Magnetic ordering in $EuRh_2As_2$ studied by x-ray resonant magnetic scattering

S. Nandi,[1] A. Kreyssig,[1] Y. Lee,[1] Yogesh Singh,[1] J. W. Kim,[2] D. C. Johnston,[1] B. N. Harmon,[1] and A. I. Goldman[1]
[1]*Ames Laboratory, US DOE and Department of Physics and Astronomy, Iowa State University, Ames, Iowa 50011, USA*
[2]*Advanced Photon Source, Argonne National Laboratory, Argonne, Illinois 60439, USA*

(Received 5 February 2009; published 27 March 2009)

Element-specific x-ray resonant magnetic scattering investigations were performed to determine the magnetic structure of Eu in $EuRh_2As_2$. In the temperature range from 46 K down to the lowest achievable temperature of 6 K, an incommensurate antiferromagnetic (ICM) structure with a temperature-dependent propagation vector $\tau \approx (0\ 0\ 0.9)$ coexists with a commensurate antiferromagnetic (CM) structure. Angular-dependent measurements of the magnetic intensity indicate that the magnetic moments lie in the tetragonal basal plane and are ferromagnetically aligned within the **a**-**b** plane for both magnetic structures. The ICM structure is most likely a spiral-like magnetic structure with a turn angle of ~162° (0.9π) between adjacent Eu planes in the **c** direction. In the CM structure, this angle is 180°. These results are consistent with band-structure calculations which indicate a strong sensitivity of the magnetic configuration on the Eu valence.

DOI: 10.1103/PhysRevB.79.100407 PACS number(s): 75.25.+z, 75.30.Mb, 75.40.Cx, 75.50.Ee

The complex interplay among superconductivity, magnetism, and structural instabilities in AFe_2As_2 (A=Ba, Sr, Ca, and Eu) pnictides upon chemical substitution or under applied pressure has generated a great deal of recent attention and research activity.[1–7] Related isostructural compounds such as $BaRh_2As_2$, $BaMn_2As_2$, and $EuRh_2As_2$ (Refs. 8–10) have also been synthesized and studied in an attempt to increase significantly superconducting transition temperatures and to understand the role of Fe in the Fe-As layers as well as the A site in promoting superconductivity. The metallic compound $EuRh_2As_2$ shows a plethora of interesting physical properties such as giant magnetoresistance and a strong reduction in the electronic specific-heat coefficient with applied field in the antiferromagnetic state.[10] The reported intermediate valence of 2.13(2) for Eu (Ref. 10) adds further interest as it may be tuned by applied pressure or temperature.[11,12] Since Eu^{2+} ions carry a magnetic moment with spin $S=7/2$ while Eu^{3+} does not have a permanent magnetic moment, $EuRh_2As_2$ may be an excellent model system to study the complex interplay between valence and magnetism in the "122" pnictides.

$EuRh_2As_2$ crystallizes in the $ThCr_2Si_2$-type tetragonal structure with space group $I4/mmm$ (Ref. 13) and lattice parameters $a=4.075$ Å and $c=11.295$ Å at $T=298$ K.[10] Specific-heat and magnetization data indicate that the Eu moments order antiferromagnetically below $T_N=46$ K.[10] The magnetic susceptibility parallel to the **c** axis increases below T_N and decreases when measured perpendicular to the **c** axis.[10] This indicates that the moments are primarily aligned in the basal **a**-**b** plane. Nevertheless, the microscopic details of the magnetic structure are, as yet, unknown. Here, we report on the magnetic ordering of Eu moments in $EuRh_2As_2$ studied by x-ray resonant magnetic scattering (XRMS).[14] For the present measurements, this technique offers several advantages over neutron scattering due to the large neutron absorption cross section of the natural isotope ^{152}Eu. Moreover, the elemental specificity and superior wave-vector resolution provided by x rays can be employed to determine precisely the magnetic propagation vector, particularly for systems with more than one propagation vector.

Single crystals of $EuRh_2As_2$ were grown using Pb flux.[10] For the XRMS measurements, an as-grown platelike single crystal with a surface perpendicular to the **c** axis and of approximate dimensions $1\times1\times0.1$ mm^3 was selected. The sample shows very similar magnetic behavior to that recently reported.[10] The XRMS experiment was performed on the 6ID-B beamline at the Advanced Photon Source at the Eu L_{II} absorption edge ($E=7.611$ keV). The incident radiation was linearly polarized perpendicular to the vertical scattering plane (σ polarized) with a spatial cross section of 1.0 (horizontal) $\times 0.25$ mm^2 (vertical). In this configuration, resonant magnetic scattering rotates the plane of linear polarization into the scattering plane (π polarization).[14] In contrast, charge scattering does not change the polarization of the scattered photons (σ-σ scattering). Pyrolytic graphite (PG) (0 0 6) was used as a polarization and energy analyzer to suppress the charge and fluorescence background relative to the magnetic scattering signal. The sample was mounted at the end of the cold finger of a displex cryogenic refrigerator with the **a**-**c** plane coincident with the scattering plane and was measured at temperatures between 6 and 50 K.

Figure 1 shows a scan along the [0 0 1] direction, measured at the peak of the dipole resonance (Fig. 2) at an x-ray energy $E=7.614$ keV in the rotated σ-π channel. At $T=6$ K$<T_N$, other than the allowed charge reflections $(0\ 0\ L)$ with L=even, satellite peaks appear which can be indexed as $(0\ 0\ L)\pm\tau$ with $\tau\approx(0\ 0\ 0.9)$, indicating an incommensurate

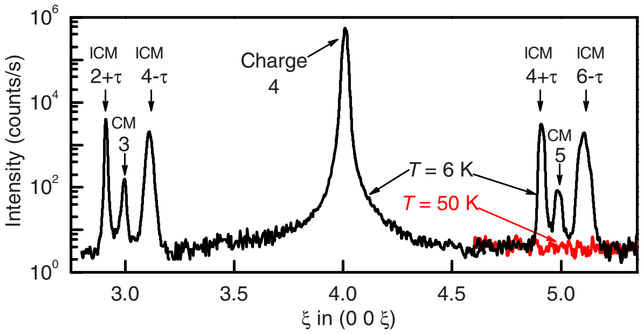

FIG. 1. (Color online) Scan along the [0 0 1] direction at $T=6$ K in the rotated σ-π channel. Note that the intensity is shown on a logarithmic scale. The data around (0 0 5) are shown at $T=50$ K$>T_N$ for comparison.

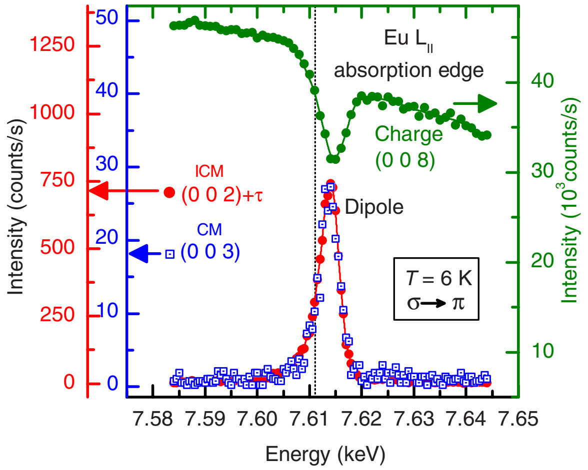

FIG. 2. (Color online) Energy scans of the ICM $(0\ 0\ 2)+\tau$ and CM (0 0 3) reflections and of the charge (0 0 8) reflection. The vertical line depicts the Eu L_{II} absorption edge as determined from the inflection point of the charge signal. The solid lines are guides to the eyes.

magnetic (ICM) structure. There are also weak peaks at $(0\ 0\ L)$ with L=odd pointing to an additional commensurate magnetic (CM) structure with propagation vector (0 0 1).[15] Careful scans along the [100] and [110] directions reveal no additional satellite peaks.[16] To confirm the resonant magnetic behavior of these peaks, we performed energy scans through the Eu L_{II} absorption edge in the σ-π channel (shown in Fig. 2) at 6 K.[17] We observed one resonance peak approximately 3.5 eV above the absorption edge for both ICM and CM structures. This peak arises from dipole resonant scattering involving transitions between the core $2p$ and the empty $5d$ states[14] and confirms that Eu is magnetic in EuRh$_2$As$_2$. No quadrupole resonance ($2p$ to $5d$) signal was detected, which would have appeared a few eV below the absorption edge.

Figure 3(a) shows the temperature dependence of the integrated intensity of the ICM $(0\ 0\ 6)+\tau$ and $(0\ 0\ 8)-\tau$ satellite peaks, and the CM (0 0 3) Bragg reflection. The smooth variation in magnetic intensity close to the transition temperature indicates that the phase transition is second order. The integrated intensity ($I \sim \mu^2$, where μ is the sublattice magnetization[18]) can be fitted with a power law of the form $I \sim (1-\frac{T}{T_N})^{2\beta}$. The obtained exponents $\beta = 0.32 \pm 0.02$ and $\beta = 0.7 \pm 0.1$ for the ICM and CM peaks, respectively, will be discussed later. The measured transition temperature, $T_N = 46.0 \pm 0.5$ K, is in excellent agreement with the value $T_N = 46 \pm 1$ K determined from the magnetization and heat-capacity measurements.[10] Figure 3(b) shows the temperature dependence of the propagation vector after correcting for the thermal expansion of the lattice. The propagation vector varies smoothly from (0 0 0.905) at 6 K to (0 0 0.885) at 46 K, supporting further the incommensurate nature of the ICM structure.

We now turn to the determination of the magnetic moment configuration. For the crystallographic space group $I4/mmm$ and propagation vectors of the form $(0\ 0\ \tau)$, two independent magnetic representations are possible with moments that are either strictly along the **c** direction or confined to the **a**-**b** plane.[19] For a second-order phase transition, Landau theory predicts that only one of the two above-mentioned representations is realized at the phase transition.[19] To differentiate between these two representations, a series of CM and ICM Bragg reflections were measured. Figure 4(a) shows the expected angular dependence of the magnetic intensity for the two above-mentioned representations along with the observed intensities. The XRMS intensity for the current experimental configuration can be calculated as[20]

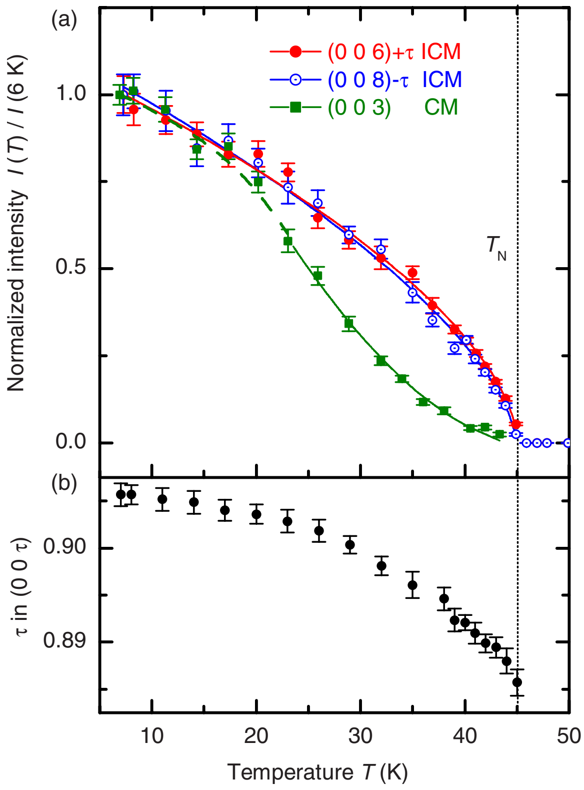

FIG. 3. (Color online) (a) Temperature dependence of the integrated intensity of the pair of ICM $(0\ 0\ 6)+\tau$ and $(0\ 0\ 8)-\tau$ satellite peaks and of the CM (0 0 3) Bragg reflection determined by fitting θ-2θ scans with a Lorentzian function. The solid lines are fit to the data as described in the text and the dashed line is a guide to the eyes. (b) Temperature dependence of the propagation vector as determined from the pair of ICM reflections.

$$\begin{aligned} I &= B\frac{(\mu_a \cos\theta)^2}{\sin 2\theta}, \quad \text{for } \mu \text{ in the } \mathbf{a}\text{-}\mathbf{b} \text{ plane} \\ &= B\frac{(\mu_c \sin\theta)^2}{\sin 2\theta}, \quad \text{for } \mu \parallel \mathbf{c}, \end{aligned} \tag{1}$$

where B is a scaling factor, θ is the Bragg angle, $1/\sin 2\theta$ is the Lorentz factor, and μ_a and μ_c are the components of magnetic moments along the **a** and **c** directions, respectively. Since the model calculation with the magnetic moment in the **a**-**b** plane closely agrees with the observed intensity, we conclude that the magnetic moments lie in the **a**-**b** plane for both the ICM and CM structures.

Both a transverse amplitude modulated collinear antifer-

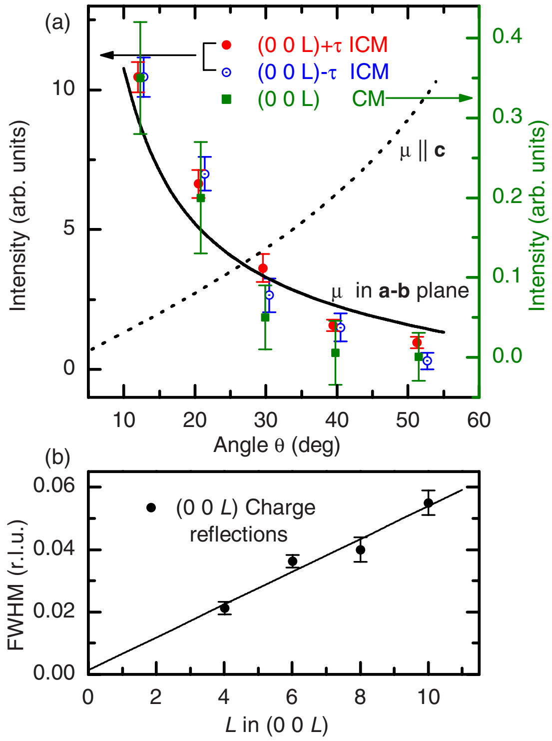

FIG. 4. (Color online) (a) Angular dependence of the integrated intensity of the ICM (0 0 L)+τ and (0 0 L)-τ satellite peaks with L being even and of the CM (0 0 L) Bragg reflections with L being odd. The solid and dotted lines represent expected angular dependence for moments in the **a-b** plane and in the c direction, respectively. (b) L dependence of the FWHM of a series of (0 0 L) charge reflections. The solid line represents the expected L dependence for a sample with variation in lattice parameter (Ref. 21).

romagnetic structure and a basal plane spiral antiferromagnetic structure are consistent with moments in the **a-b** plane and a propagation vector of (0 0 0.9). In an XRMS experiment one cannot distinguish between these two structures due to the presence of domains. However, we note that a spiral-like structure can persist down to the lowest temperature whereas a transverse amplitude modulated magnetic structure must transform to a square-wave modulation due to the expected equal amplitude of ordered magnetic moments at low temperatures. Such a "squaring up" of the magnetic structure would produce third harmonic satellite peaks, $\pm 3\tau$, at $T=6$ K, which were not observed (see Fig. 1). Therefore, we conclude that the ICM structure is a spiral-like structure with ferromagnetically coupled moments in each **a-b** plane and a temperature-dependent turn angle of $\sim 162°(0.9\pi)$ between adjacent Eu planes. For the CM structure, the magnetic moments are also ferromagnetically aligned within the **a-b** plane. The observation of CM Bragg reflections at (0 0 L) with L odd, together with the absence of a ferromagnetic signal in magnetization measurements,[10] indicates that the magnetic moments in the adjacent Eu planes are collinearly aligned in opposite directions for the CM structure.

We now turn to the discussion of certain subtle features observed in the XRMS study. First of all, from Fig. 1, we note that the full width at half maximum (FWHM) for pairs of satellite reflections, for example, $(0\ 0\ 4)\pm\tau$, is quite different and there is an overall increase in FWHM with increasing scattering angle. Such features in FWHM for scans along the [0 0 1] direction can be explained assuming a variation in the lattice parameter $\Delta c \sim 0.05$ Å and a related variation in the propagation vector $\Delta\tau \sim (0\ 0\ 0.03)$. Simultaneous variations in both **c** and τ compensate each other for the positions of the $+\tau$ satellite peaks and result in an unchanged FWHM. The effect is opposite for the $-\tau$ satellites, yielding a strong variation in the positions for the $-\tau$ satellites and, therefore, increasing the FWHM significantly. The variation in lattice parameter in the sample is also evident from the linear increase in FWHM of different charge peaks as a function of L [see Fig. 4(b)] as $\Delta L \approx \frac{\Delta c}{c} L$ yielding $\Delta c \sim 0.05$ Å. Here we note that effects other than the variation in lattice parameter, such as strain, also affect the FWHM as a function of scattering angle.

Next, we turn to the observed coexistence of ICM and CM structures over the investigated temperature range. In rare-earth intermetallic systems a coexistence of CM and ICM structures is rare[22,23] and can arise from minority phases due to strain, disorder, and/or slightly varying stoichiometry in the sample. The absence of satellite reflections with a combination of both propagation vectors suggests that the two magnetic structures are independent. The intensity of the CM peaks is approximately 2 orders of magnitude lower than the ICM peaks and indicates a similar ratio in volume fractions for the CM and ICM phases. In the case of Eu-based intermetallic compounds such as EuPd$_2$Si$_2$ and EuCu$_2$Si$_2$, a minor phase has been observed which also orders magnetically at low temperatures with a slightly lower Eu valence than the main phase.[24–26]

To further investigate the effect of the Eu valence on magnetic ordering, we have performed band-structure calculations of the generalized susceptibility $\chi(\mathbf{q})$ for different valences of Eu by varying the Fermi energy. In the $\chi(\mathbf{q})$ calculation each small tetrahedron contribution (in **q** space) was weighted by the Eu 5d wave function components which are predominantly responsible for coupling the Eu 4f moments via the Ruderman-Kittel-Kasuya-Yosida (RKKY) mechanism. We employed the full-potential linearized augmented plane-wave (LAPW) method to treat the 4f-5d exchange adequately. It was used with $R_{\mathrm{MT}}K_{\max}=8$ and $R_{\mathrm{MT}}=2.5$, 2.2, and 2.2 a.u. for Eu, Rh, and As, respectively, 405 k points in the irreducible Brillouin zone for the self-consistent charge, and 34 061 k points in the whole reciprocal unit cell for the $\chi(\mathbf{q})$ calculations. For the local density functional, the Perdew-Wang 1992 functional[27] was employed. The convergence criterion for the total energy was 0.01 mRy/cell.

In Fig. 5, a distinct peak is evident in $\chi(\mathbf{q})$ at $\mathbf{q}=(0\ 0\ 1)$ for divalent Eu and the peak moves progressively to lower values of **q** as the valence is increased (see inset to Fig. 5 for details). We note the presence of additional local maxima around $\mathbf{q}=(0\ 0\ 0.6)$ and the zone center. Rather than attempt a detailed treatment of RKKY matrix elements, we have calculated the total energy of the virtual crystal with Eu$^{+2.1}$ for ferromagnetic ($\mathbf{q}=0$) and antiferromagnetic [$\mathbf{q}=(0\ 0\ 1)$] orderings and find that the CM phase is 9.0 meV lower in energy, thus eliminating $\chi(\mathbf{q}=0)$ peak from consideration. Therefore, band-structure calculations together with the rela-

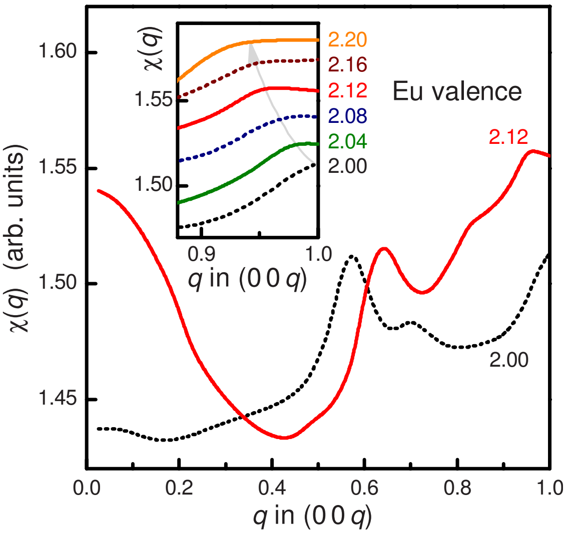

FIG. 5. (Color online) The generalized susceptibility $\chi(\mathbf{q})$ for different valence of Eu in EuRh$_2$As$_2$. The inset shows an expanded view of $\chi(\mathbf{q})$ close to the Brillouin zone boundary at $\mathbf{q}=(0\ 0\ 1)$.

tively weak intensity of the CM peaks suggest that the CM structure originates from a minor phase associated with the divalent Eu ions and the ICM structure from the major phase with an average valence of 2.13(2), as inferred from the magnetization measurement.[10]

We note that the temperature dependence of the CM peak is quite different from the temperature dependence of the ICM peaks, and the value of the critical exponent is twice that of the ICM peak. For the ICM peaks, the value of the critical exponent (β=0.32) is close to that (β=0.36) (Ref. 28) of the three-dimensional (3D) classical Heisenberg model, typical for rare-earth elements in intermetallic compounds.[18] As the temperature dependence of surface magnetism ($\beta \approx 0.7$) (Ref. 29) can be quite different than in the bulk, a surface bias of the minority phase could explain the difference in the temperature dependences.

In summary, we have determined that below 46 K an ICM structure with a temperature-dependent propagation vector $\tau \approx (0\ 0\ 0.9)$ coexists with a minor CM structure for the magnetic order of Eu in EuRh$_2$As$_2$. The magnetic moments for both the ICM and CM structures are within the tetragonal **a-b** plane and are ferromagnetically aligned within this plane. For the ICM structure, a spiral-like structure is most likely with a turn angle of 162° between moments in adjacent Eu planes. The existence of a spiral-like ICM structure down to the lowest temperature indicates a weak in-plane anisotropy. For the CM structure, magnetic moments in the adjacent Eu planes are antiparallel aligned. Simultaneous occurrence of both the ICM and CM structures and a different temperature dependence of the CM peak can be explained with an additional minor phase and is consistent with $\chi(\mathbf{q})$ calculations, showing a strong sensitivity on the Eu valence. Band-structure calculations together with the observed coexistence of CM and ICM phases indicate a delicate energy balance between different magnetic configurations in EuRh$_2$As$_2$ and make this compound a promising candidate for studying the complex interplay between changes in valence and magnetism as a function of external parameters.

We thank D. S. Robinson for his help during experiments. The work at the Ames Laboratory and at the MU-CAT sector was supported by the U.S. DOE under Contract No. DE-AC02-07CH11358. Use of the Advanced Photon Source was supported by U.S. DOE under Contract No. DE-AC02-06CH11357.

---

[1] M. Rotter *et al.*, Phys. Rev. Lett. **101**, 107006 (2008).
[2] N. Ni *et al.*, Phys. Rev. B **78**, 014507 (2008).
[3] K. Sasmal *et al.*, Phys. Rev. Lett. **101**, 107007 (2008).
[4] P. L. Alireza *et al.*, J. Phys.: Condens. Matter **21**, 012208 (2009).
[5] M. S. Torikachvili *et al.*, Phys. Rev. Lett. **101**, 057006 (2008).
[6] A. Kreyssig *et al.*, Phys. Rev. B **78**, 184517 (2008).
[7] A. I. Goldman *et al.*, Phys. Rev. B **79**, 024513 (2009).
[8] Y. Singh *et al.*, Phys. Rev. B **78**, 104512 (2008).
[9] Y. Singh *et al.*, arXiv:0901.3370, Phys. Rev. B (to be published).
[10] Y. Singh *et al.*, arXiv:0902.0352 (unpublished).
[11] J. Röhler *et al.*, Phys. Rev. Lett. **49**, 65 (1982).
[12] M. Chefki *et al.*, Phys. Rev. Lett. **80**, 802 (1998).
[13] A. Hellmann *et al.*, Z. Naturforsch., B: Chem. Sci. **62b**, 155 (2007).
[14] J. P. Hannon *et al.*, Phys. Rev. Lett. **61**, 1245 (1988).
[15] The propagation vectors (0 0 1) and (1 0 0) are equivalent for the space group $I4/mmm$. A magnetic structure or superstructure with such propagation vectors breaks the symmetry relations given by the body center.
[16] $(\xi\ 0\ 8)$ $(0\ \xi\ 8)$, and $(\xi\ \xi\ 8)$ scans were performed with appropriate range and step size of ξ and a counting time of 4 s for each data point.
[17] It was necessary to attenuate the incident beam by 75% to reduce beam heating, to properly characterize the temperature dependence of integrated intensity, and to determine the transition temperature. Measurements shown in Figs. 2–4 are performed with this attenuation.
[18] T. Brückel *et al.*, Eur. Phys. J. B **19**, 475 (2001).
[19] A. S. Wills, Physica B **276-278**, 680 (2000).
[20] J. P. Hill *et al.*, Acta Crystallogr. **52**, 236 (1996).
[21] The FWHM in scans along the [0 0 1] direction is dominated by the variation in the c lattice parameter and is an order of magnitude larger than the intrinsic FWHM, as is evident from the linear extrapolation of FWHM to small L values.
[22] J. P. Hill *et al.*, Phys. Rev. B **53**, 3487 (1996).
[23] A. Llobet *et al.*, Phys. Rev. Lett. **95**, 217002 (2005).
[24] M. M. Abd-Elmeguid *et al.*, J. Phys. C **18**, 345 (1985).
[25] E. Holland-Moritz *et al.*, Phys. Rev. B **35**, 3122 (1987).
[26] E. R. Bauminger *et al.*, Phys. Rev. Lett. **30**, 1053 (1973).
[27] J. P. Perdew *et al.*, Phys. Rev. B **45**, 13244 (1992).
[28] F. Kagawa *et al.*, Nature (London) **436**, 534 (2005).
[29] G. M. Watson *et al.*, Phys. Rev. Lett. **77**, 751 (1996).